THE JOURNAL OF PHYSICAL CHEMISTRY C

pubs.acs.org/JPCC Article

Understanding Excitonic Behavior in Light Absorption and Recombination Process

Bolin Guo, Chao Luo, Cheng Yan, Bai Sun,* Wen Li,* and Weiqing Yang*

Cite This: J. Phys. Chem. C 2020, 124, 26076−26082 Read Online

ACCESS | Metrics & More | Article Recommendations | Supporting Information

ABSTRACT: Understanding excitonic behavior in light absorption and recombination process is urgently needed to regulate luminescent properties of two-dimensional (2D) perovskite; however, such information is still unexplored. Here, first, we demonstrate that pure phenethylamine lead bromine (PEA_2PbBr_4) nanosheets (NSs) possess strong exciton absorption and emission spectrum with high exciton binding energy (up to 310 meV) and prove that free excitons (FEs) play a decisive role in the optical transition process. Then, we design Cd-doped PEA_2PbBr_4 NSs to induce self-trapped excitons (STEs). Doping with isoelectric Cd naturally induces an impurity-driven lattice distortion and a strong exciton−phonon coupling, resulting in the STEs broadband extrinsic luminescence spectra. Further, the corresponding exciton fluorescent components of FEs and STEs can be effectively distinguished from the emission spectrum through spectral line-shape analysis, revealing the synergistic effect of exciton states in the recombination process. Unambiguously, this work will provide a deeper understanding of the exciton behavior and look forward to regulating exciton composition to obtain ideal luminescence properties.

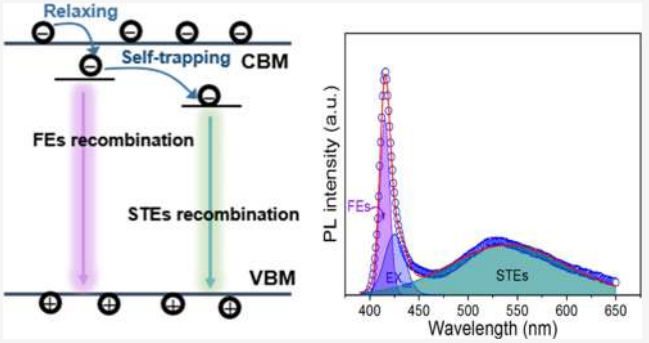

1. INTRODUCTION

Hybrid organic−inorganic perovskites naturally possess a rich structure and morphology, including zero-dimensional (0D) quantum dots, one-dimensional (1D) nanowires, and two-dimensional (2D) NSs, which has received a lot of attention from scientific and industrial communities.[1−6] As an emerging semiconductor material, they have already demonstrated exceptional potential applications in solar cells, light-emitting diodes (LEDs), photodetectors, and lasers.[7−12] Among them, 2D layered perovskites exhibit long-term stability owing to their atomically layered thickness and abundant surface ligands, arousing great concern of the scientific community. 2D perovskite could be divided into three categories, including Dion−Jacobson (DJ) phase, Ruddlesden−Popper (RP) phase, and cation-alternated interlayer space (ACI) phase.[13] Among them, the widely studied RP phase 2D perovskites have a general composition $R_2A_{n-1}B_nX_{3n+1}$ (R is the organic cation, A is the central cation, B is the metal cation, X is the halide, n is the number of octahedral layers),[14] in which adjacent octahedral layers are separated by large organic cation R and the optical and electrical properties change with the number of layers.

2D perovskite NSs have been demonstrated to have exceptional photophysical properties due to their natural quantum-well structure and analogous excitonic behaviors, such as large exciton binding energy (E_b), exciton resonance, and exciton photoluminescence (PL) emission,[15] while the luminescent properties of the perovskite strongly rely on these exciton behaviors. Further, these excitonic behaviors can intrinsically control the light absorption−recombination process. Therefore, understanding the intrinsic exciton absorption and recombination behavior to regulate the luminescence mechanism is essential for the desirable fluorescence properties.[16] Generally speaking, exciton recombination of the 2D perovskite usually includes free exciton (FEs) recombination and self-trapped exciton (STEs) recombination. FEs can move freely in the crystal space, while the STEs are bound electron−hole pairs localized in the potential well due to lattice distortion, the most obvious feature for STEs is the wideband luminescence phenomenon. Typically, the mutual transformation of FEs and STEs will lead to the overlap of the luminescence spectra.[17,18] To reveal the excitonic behavior in the recombination process, it is necessary to distinguish the luminescent components of the corresponding composite carriers, but such important information is still rare in the literature.

Received: October 14, 2020
Revised: October 31, 2020
Published: November 13, 2020

https://dx.doi.org/10.1021/acs.jpcc.0c09334
J. Phys. Chem. C 2020, 124, 26076−26082

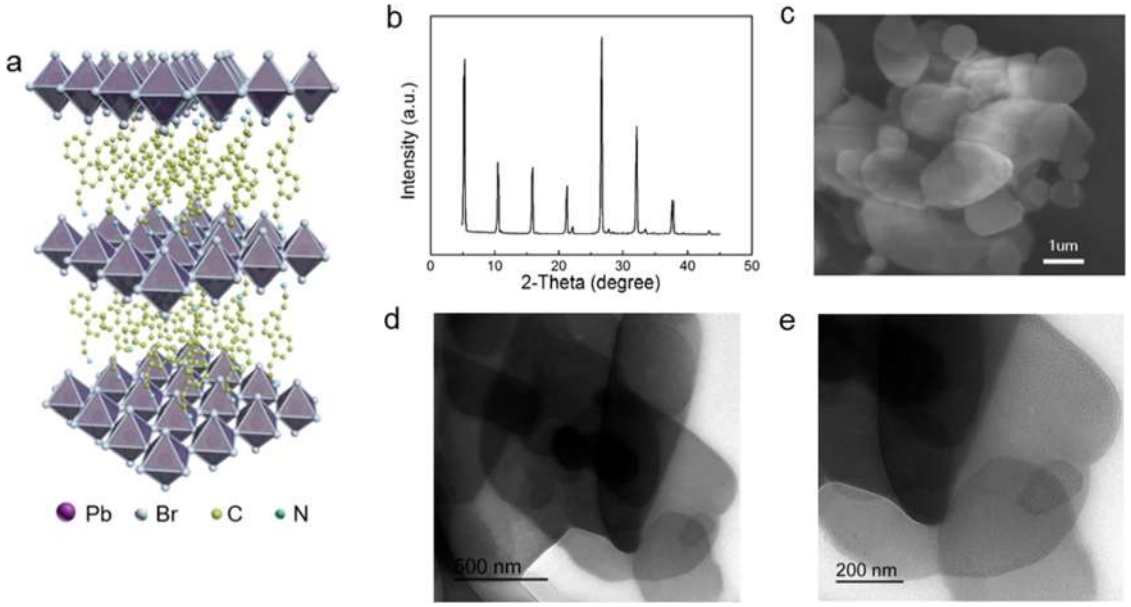

Figure 1. Structure and characterization of 2D PEA_2PbBr_4 NSs. (a) Structure diagram of 2D PEA_2PbBr_4 NSs. The adjacent octahedral layers are separated by phenylethylamine ligands. (b) X-ray diffraction (XRD) patterns of PEA_2PbBr_4. (c–e) SEM images and TEM images of PEA_2PbBr_4 NSs.

In this work, we clearly demonstrate the 2D excitonic behaviors of pure PEA_2PbBr_4 perovskite NSs through the Elliot Theory. Also, from the linear dependence of integrated intensity on excitation density, we found that the emission spectra are completely ascribed to FE recombination. Moreover, we design Cd-doping PEA_2PbBr_4 perovskite NSs to induce STEs. The generation of STEs is attributed to the impurity-driven lattice distortion and a strong exciton–phonon coupling. Moreover, through spectral line-shape analysis, the corresponding excitonic fluorescent components of FEs and STEs could be effectively identified to reveal excitonic behavior in the recombination process. Therefore, this work can shed light on how to regulate exciton behavior to control the optical properties of the optoelectronic devices of novel 2D materials.

2. EXPERIMENTAL SECTION

2.1. Materials. Oleic acid (90%, OA), 1-octadecene (90%, ODE), lead acetate (99.99%, $Pb(Ac)_2$-$2H_2O$), phenylethylamine (98%, PEA), hydrobromic acid (HBr, 48%), and cadmium acetate ($Cd(Ac)_2$-$2H_2O$, 99.99%) were purchased from Shanghai Aladdin Industrial Corporation Co., Ltd. *n*-Hexane (99.5%) was purchased from Beijing Chemical Factory. The water of crystallization of $Pb(Ac)_2$–$2H_2O$ and $Cd(Ac)_2$–$2H_2O$ was evaporated by baking in a vacuum at 80 °C. All of the chemicals are used directly without further purification.

2.2. Synthesis of PEA_2PbBr_4 Perovskite Crystal. PEA_2PbBr_4 NSs were synthesized according to the previous literature but made some modification,[19] 10 mL of ODE, 1 mL of OA, 150 μL of PEA, and 0.0758 g of $Pb(Ac)_2$ were load in a 100 mL three-necked round-bottom flask. Then, the flask was vacuumed at 100 °C for 20 min; after that, the flask was switched to N_2 and temperature was increased to 140 °C and 1 mL of HBr was quickly injected into the three-necked flask. An ice-water bath was immediately applied to cool the solution after injection. The as-prepared solution was subjected to centrifugation at 6000 rpm for 8 min to discard the supernatant containing unreacted precursor and byproducts; after that, 10 mL of *n*-hexane was added into the precipitate and then centrifuged at 6000 rpm for 8 min. After that, the precipitate was dispersed in 10 mL of *n*-hexane to form a stable colloidal solution.

2.3. Synthesis of Cd-Doped PEA_2PbBr_4 Perovskite Crystal. The synthetic process of the Cd-doped PEA_2PbBr_4 nanosheets was similar to that of the pure PEA_2PbBr_4 nanosheets, just adding different ratios of $Cd(Ac)_2$ during the synthesis process, the addition of $Cd(Ac)_2$ are 0.3, 0.9, 3.6, 5.3 mg, about to 0.5, 1.6, 6.7, 9.8% doping content.

2.4. Material Characterization. The crystal structure and phase composition were determined by the XPert Pro (Holland) X-ray diffractometer with Cu Kα radiation (λ = 0.154 nm). The crystal structure and grain size were determined using a transmission electron microscope (TEM) (FEI Tecnai G2 F20) with an acceleration voltage of 200 kV. The UV absorption spectrum was obtained by UV-2500 (Shimadzu Corporation); the photoluminescence and photoluminescence excitation were investigated at room temperature using FLS980 (Edinburgh Instruments) spectrometer with a 450 W Xenon lamp. Time-resolved PL spectra were also carried out by an Edinburgh FLS980 fluorescence spectrometer with a time-correlated single-photon counting (TCSPC) spectrometer and the excitation wavelength was located at 405 nm.

3. RESULTS AND DISCUSSION

PEA_2PbBr_4 perovskite NSs possess unique properties and remarkable luminescent efficiency, making it a perfect object for studying exciton properties. Figure 1a shows the schematic illustration of PEA_2PbBr_4, in which layered lead halide octahedron is sandwiched by a PEA organic ligand on the surface. As presented in Figure 1b, it is obvious that the strong (001) diffraction peaks exist periodically and the 2D characteristic peak is located at around 5°, showing the high orientation of 2D perovskite.[20] Scanning electron microscopy (SEM) and transmission electron microscopy (TEM) images clearly show extremely thin and transparent NSs, and the

https://dx.doi.org/10.1021/acs.jpcc.0c09334
J. Phys. Chem. C 2020, 124, 26076–26082

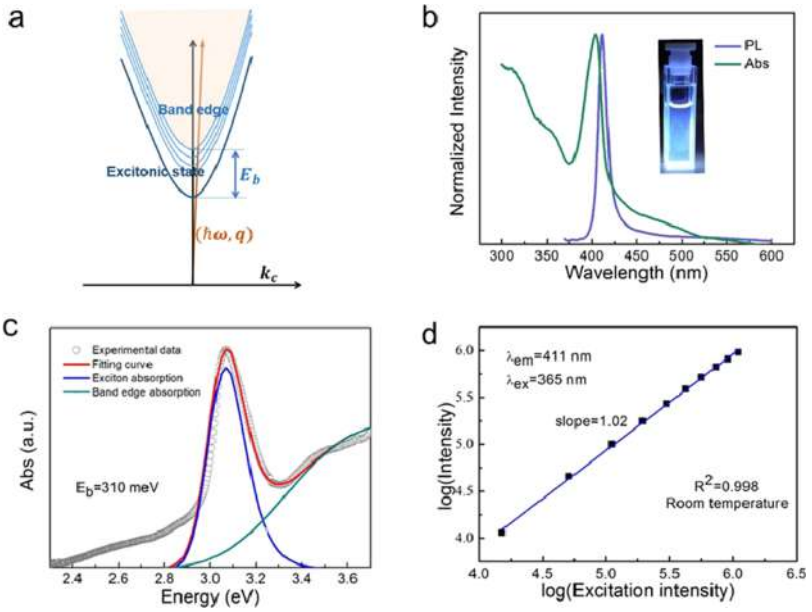

Figure 2. Exciton state and exciton behavior of pure PEA_2PbBr_4. (a) Energy dispersion curves of exciton levels. The vertical and horizontal axes are the energy (E) and wave vector (K), respectively. The origin point (0, 0) indicates the ground state. The blue parabolic curves and the sky blue parabola represent the exciton state and band edge continuous state, respectively. The orange arrow represents the phonon line with energy $\hbar\omega$ and momentum q. Since perovskite is a direct band gap semiconductor, the phonon is not involved in the optical transition; so, the phonon line is almost along the $k = 0$ axis. The gap between the lowest exciton state and the bottom of the continuum is defined as the exciton binding energy E_b. (b) PL spectrum and absorption spectra of PEA_2PbBr_4, and the inset is the photographs of NS solution illuminated under a 365 nm ultraviolet lamp. (c) Measured absorption spectrum and its corresponding fitting curve based on the quantum-well absorption model of the Elliott Theory. (d) Double logarithm fitting curve of the power-dependent emission intensity at room temperature.

lateral dimension can reach micron levels (Figure 1c–e). Such an ultrathin nanosheet can result in a strong spatial confinement effect in the vertical direction, which makes it easier to generate excitons due to the mutual attraction of free carriers (electrons and holes).

Excitons, an important feature of the 2D photoelectric materials, exert a significant effect on the photophysical properties.[21] Usually, excitons can be divided into two categories, namely, Frankel excitons and Wannier excitons. Frankel excitons are often found in insulators and tightly bound electron–hole pairs with small exciton Bohr radius, while Wannier excitons are called large excitons (the distance between electron holes is larger than the lattice constant) with a weak binding force.[22] However, for lead halide perovskite semiconductors, we only consider the Winner exciton type.[23] The basic exciton parameters include exciton resonance and exciton binding energy. The former dominates the band edge absorption onset, while the latter is a reflection of the Coulomb interaction energy between photoexcited electrons and holes. The generated excitonic state is ascribed to the overlapping of electron and hole wave functions under strong confinement effect according to the exciton Schrodinger equation.[24] Excitonic states emerge as a series of discrete energy levels under continuous conduction band edge and are also known as the exciton Rydberg series.[25] E_b is defined as the energy difference between the exciton ground state level and the conduction band edge. As shown in Figure 2a, the relationship between the exciton state and the conduction band edge can be described by the dispersion curve. Noted, to satisfy the transition energy and momentum selection rules, the optical transition is allowed only when the phonon line and dispersion curve intersect.

For clearly revealing the influence of the excitonic state on the external luminescence spectrum, the photoluminescence (PL) spectrum, absorption spectra, and time-resolved PL (TRPL) of 2D PEA_2PbBr_4 NSs were measured. Due to the strong confinement effect of the 2D perovskite, they exhibit a narrow emission spectrum located at 413 nm and a strong exciton absorption peak near 406 nm (Figure 2b). The PL line shape is asymmetric with a slight emission tail in the long wave region, which may have originated from the localization of excitons.[26] Accordingly, full width at half-maximum (FWHM) of the PL spectra is only 12.9 nm, the Stokes shift is 7.45 nm, and the fitting average lifetime from the TPRL spectrum is 0.54 ns (Figure S1), showing the superfast femtosecond level recombination rate of FEs.[27] Such an obvious approximate coincidence of the exciton absorption and emission peak can evidently indicate that the excitonic state should play a decisive role in the recombination process.

These existing excitonic states will greatly affect the transition from the ground state to the excited state especially when the photon energy is less than the band gap (E_g). Using quantum-well absorption model based on the Elliot Theory,[28] the absorption line of the exciton and exciton binding energies can be evaluated by fitting the absorption spectra with the exciton absorption and band edge absorption according to the following formula

$$p_E = p_x + \frac{A_c}{2}\left[\mathrm{erf}\left(\frac{(E - E_0) - E_b^x}{\gamma_c}\right) + 1\right] \quad (1)$$

$$p_x = \frac{1}{2\eta}\left[\mathrm{erf}\left(\frac{E - E_0}{\gamma} - \frac{\gamma}{2\eta}\right) + 1\right]\exp\left(\frac{\gamma^2}{4\eta^2} - \frac{E - E_0}{\eta}\right) \quad (2)$$

https://dx.doi.org/10.1021/acs.jpcc.0c09334
J. Phys. Chem. C 2020, 124, 26076–26082

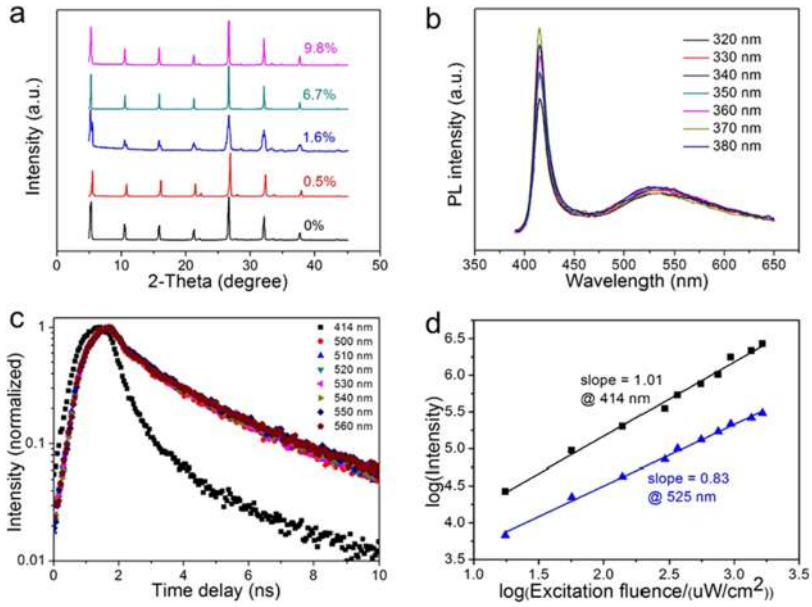

Figure 3. (a) XRD patterns of Cd-doped PEA_2PbBr_4 with different Cd-doping concentrations. (b) PL spectra under different excitation wavelengths of 6.7% doped NSs. (c) PL decay curves of PEA_2PbBr_4:Cd (6.7%) at different emission wavelengths. (d) Fluence-dependent PL intensity of PEA_2PbBr_4:Cd (6.7%). The emission wavelength is selected as 400 and 535 nm.

where p_E and p_x are the total absorption line and the exciton absorption line with asymmetric broadening η and symmetric broadening γ, respectively; A_c and γ_c are the step height and width of the continuous band edge absorption; E_0 and E_b^x are the actual exciton energy and exciton binding energy, respectively. From the band edge absorption fitting, the as-obtained E_b values for PEA_2PbBr_4 NSs is up to 310 meV (Figure 2c), which is in good agreement with previously reported large exciton binding energy.[29] Moreover, fitting excitonic absorption edge through the Kubelka–Munk formula,[30] the energy of the exciton ground state (lowest excitonic state energy) is 2.95 eV (Figure S2), so the band gap of PEA_2PbBr_4 can be inferred to be 3.26 eV (lowest excitonic state energy plus exciton binding energy). According to the power law formula $I_{PL} \sim I_{ex}^k$, the fitting power law coefficient k of the double logarithmic PL intensity–excitation efficiency curve is equal to 1 at room temperature (Figure 2d), confirming that this FE recombination mechanism.[31] Therefore, we can infer that 2D PEA_2PbBr_4 NSs should be a typical kind of exciton semiconductor, and the excitonic state should determine its absorption and recombination process.

2D perovskites have been reported repeatedly to exhibit a strong exciton–phonon coupling due to its soft lattice and polar semiconductor characteristics.[32,33] When the exciton–phonon interaction strength (Huang–Rhys factor S) exceeds the threshold value, FEs will be localized somewhere and transform into STEs.[34] As a kind of bound excitons, the STE emission spectrum usually exhibits the broadband emission phenomenon, and photon energy emitted from the bound excitons is usually lower than that from free exciton. As proved before, the optical properties of the 2D perovskites are attributed to the excitonic state. Therefore, it is extremely significant to consider its effect on the light absorption–recombination process when free excitonic state and self-trapped excitonic state coexist, while the pure PEA_2PbBr_4 does not show any signal of the STE broadband luminescence. Therefore, we introduce Cd atoms to create STEs.

The synthesis method of the Cd-doped perovskite crystals is the same as that of pure PEA_2PbBr_4 (see details in the Supporting Information). Owing to the isoelectronic properties of Cd and Pb atoms, we are able to prepare a solid solution of $PEA_2Cd_xPb_{1-x}Br_4$ with adjustable doping levels. As shown in Figure 3a, powder XRD patterns reveal that Cd-doped 2D perovskites indeed retain the phase structure, demonstrating that the introduction of the Cd atom substitutes the original Pb ion site. For the spectra of Cd-doped perovskite crystals, we observed that a narrow emission peak (FEs emission) is located at 414 nm and a broadband emission peak with a large FWHM 132.4 nm is located at 535 nm (Figure S4). Although the Cd-doped NS show wide band luminescence characteristic, a strict proof process is still needed to further determine whether broadband emission is from STEs or not. The key is to prove whether the broadband emission is devoted to the same luminous center.[35] Here, by comparing the emission spectra under different excitation wavelengths, the TRPL spectrum, and the fluence-dependent PL spectrum, we can confirm the origin of the STEs. As shown in Figure 3b–d, the broadband spectra under different excitation wavelength and time-resolution spectrum of broadband luminescence show almost the same profile. In addition, it has a longer lifetime than the free exciton emission (1.6 ns for STEs and 0.48 ns for FEs; Figures S5 and Table S1). Besides, it presents a linear relationship between the luminescence intensity and excitation flow. All the above evidence substantially suggests that the origin of the broadband luminescence should be from the STEs in our experiment.

STEs can be considered to be the basic photophysical phenomenon, which usually exists in a system with a low-dimensional electronic structure.[36] A number of previous first-principles calculation and temperature-dependent spectrum experiments have already demonstrated that the generation of STEs is closely related to the exciton–phonon coupling caused by lattice distortion,[37] but their results cannot fully describe how free carriers are captured through lattice distortion. While

https://dx.doi.org/10.1021/acs.jpcc.0c09334
J. Phys. Chem. C 2020, 124, 26076–26082

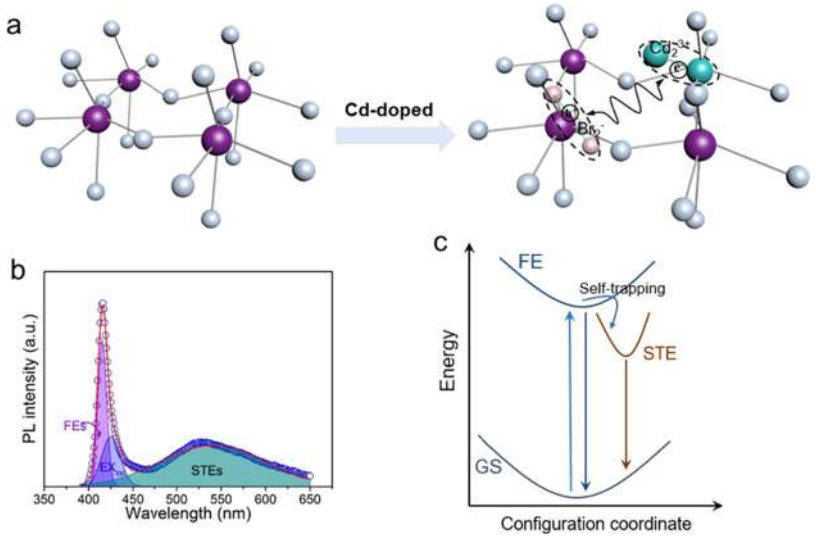

Figure 4. (a) After Cd doping. Cd_2^{3+} (cyan) and Br_2^- (pink) dimers formed through self-trapped electron and self-trapped hole, respectively. (b) PL emission spectra of 6.7% Cd-doped PEA_2PbBr_4, we can distinguish the luminescent components for host excitons (FEs and EX_{loc}) and STEs in the emission spectrum using OriginPro 9.1 Peak Analyzer tool. (c) Coordinate diagram for exciton self-trapping (blue) and FEs and STEs recombination.

in this work, we can accurately describe the excitons' self-trapping mechanism through the atomic lattice model.

First, we explained the role of Cd in inducing the formation of STEs. When Cd atoms are incorporated into the perovskite crystal, the STE recombination channel opened, proving the ability of $CdBr_6^{4-}$ octahedron to localize excitons. After Cd-doping, the lowest conduction band is composed of the 5s orbitals of Cd atoms and 6p orbitals of Pb atoms. Because the energy of the 5s orbitals is lower than that of the 6p orbital of Pb atoms, its conduction band minima are shifted to lower energy levels but the valence band maxima of the resulting perovskites remain unchanged. In this way, we can assume that lower conduction band levels provide a basis for exciton localization, and the role of Cd atoms is to trigger exciton self-trapping around the doping site and create a potential well around impurities, resulting in the formation of STEs and its subsequent broadband luminescence. The role of Cd in triggering exciton self-trapping could also be considered to cause lead bromide octahedron distortion. Usually, Jahn–Teller-like distortion is mainly responsible for the observed broadband emission, while non-Jahn–Teller-like distortion is often accompanied by smaller dipole moments and indirect transitions, which result in weak broadband emission intensity.[38] In our experiment, perovskite crystal exhibits significant broadband emission peak, so we can consider that Jahn–Teller distortion is the main cause of STEs in this article. As shown in Figure 4a, photogenerated carriers can couple with the lattice to lower the system's energy; in this process, the easily formed Cd_2^{3+} and Br_2^- dimers can capture electron and hole, respectively. Further, the trapped carriers form STEs due to Coulomb force attraction.[39] However, in the actual situation, theoretical calculations are needed to determine the trapped carrier type.

As mentioned above, two types of exciton emissions are shown in the emission spectra (Figure 4b), namely, FEs and STEs emission. As shown in Figure 4c, for the above band gap excitation from the ground state (GS), the generated free carriers quickly degenerate into FEs, and the STEs are generated through the exciton self-trapping process, which requires free excitons to overcome a certain energy barrier. Moreover, as confirmed earlier, the presence of exciton states modifies the light absorption–recombination process. However, the situation is slightly different for STEs because the self-trapped state only exists in the excited state, and the self-trapped energy level recovers due to lattice distortion recovery. Therefore, the existence of a self-trapped state only affects the recombination process of photoexcited carriers. Using the line-shape analysis for the PL spectrum of the Cd-doped perovskite crystal, we can distinguish the corresponding components for FEs and STEs. As shown in Figure 4b, PL emission spectra of Cd-doped PEA_2PbBr_4 was contributed by FEs, EX_{loc} (localized exciton) and STEs, the contribution of STEs to the total PL area is broadband luminescence region, and the other is for host exciton emission including FEs and EX_{loc}. Therefore, we can draw a reasonable conclusion that STEs and FEs jointly modify the light recombination process, which is consistent with the conclusion of the first part of this article.

4. CONCLUSIONS

In summary, we have discussed the exciton behavior of PEA_2PbBr_4 NSs in the light absorption and recombination process. It is obvious that the excitonic states play an important role in defining external luminescent properties and future optoelectronic applications. The free excitonic states determine the mentioned band gap absorption process and are responsible for the narrow emission spectrum, and the self-trapping excitonic state determines the broadband emission spectrum in the recombination process. Certainly, because the carriers lost in the nonradiative process (such as defect and exciton fluorescence quenching) cannot be measured effectively, it is difficult to accurately distinguish the proportion of different exciton states; so, more theoretical or experimental investigations should be carried out. We believe that this work will be of great benefit to modify the intrinsic exciton behavior to regulate the luminescence properties.

https://dx.doi.org/10.1021/acs.jpcc.0c09334
J. Phys. Chem. C 2020, 124, 26076–26082

■ ASSOCIATED CONTENT

Supporting Information

The Supporting Information is available free of charge at https://pubs.acs.org/doi/10.1021/acs.jpcc.0c09334.

The PLQY measurement, Tauc plot, and time-resolution spectrum of pure PEA_2PbBr_4 NSs, PL spectrum of Cd-doped perovskite NSs with different doping contents, time-resolution spectral fitting, and related parameters at different emission wavelengths (PDF)

■ AUTHOR INFORMATION

Corresponding Authors

Bai Sun − *School of Physical Science and Technology, Key Laboratory of Advanced Technologies of Materials, Ministry of Education of China, Southwest Jiaotong University, Chengdu 610031, China;* orcid.org/0000-0002-5840-509X; Email: bsun@swjtu.edu.cn

Wen Li − *Key Laboratory of Advanced Technologies of Materials (Ministry of Education), School of Materials Science and Engineering, State Key Laboratory of Traction Power, Southwest Jiaotong University, Chengdu 610031, China*; Email: liwen3337@swjtu.edu.cn

Weiqing Yang − *Key Laboratory of Advanced Technologies of Materials (Ministry of Education), School of Materials Science and Engineering, State Key Laboratory of Traction Power, Southwest Jiaotong University, Chengdu 610031, China;* orcid.org/0000-0001-8828-9862; Email: wqyang@swjtu.edu.cn

Authors

Bolin Guo − *Key Laboratory of Advanced Technologies of Materials (Ministry of Education), School of Materials Science and Engineering, State Key Laboratory of Traction Power and School of Physical Science and Technology, Key Laboratory of Advanced Technologies of Materials, Ministry of Education of China, Southwest Jiaotong University, Chengdu 610031, China*

Chao Luo − *Key Laboratory of Advanced Technologies of Materials (Ministry of Education), School of Materials Science and Engineering, State Key Laboratory of Traction Power, Southwest Jiaotong University, Chengdu 610031, China*

Cheng Yan − *Key Laboratory of Advanced Technologies of Materials (Ministry of Education), School of Materials Science and Engineering, State Key Laboratory of Traction Power, Southwest Jiaotong University, Chengdu 610031, China*

Complete contact information is available at: https://pubs.acs.org/10.1021/acs.jpcc.0c09334

Notes

The authors declare no competing financial interest.

■ ACKNOWLEDGMENTS

This work is supported by Young Scientific and Technological Innovation Research Team Funds of Sichuan Province (Nos. 20CXTD0106 and 2019YFG0292), the Fundamental Research Funds for the Central Universities of China (A0920502051619-72), and the Sichuan Science and Technology Program (2020YJ0086).

■ REFERENCES

(1) Leng, M.; Yang, Y.; Zeng, K.; Chen, Z.; Tan, Z.; Li, S.; Li, J.; Xu, B.; Li, D.; Hautzinger, M. P.; et al. All-Inorganic Bismuth-Based Perovskite Quantum Dots with Bright Blue Photoluminescence and Excellent Stability. *Adv. Funct. Mater.* **2018**, *28*, No. 1704446.

(2) Zhou, H.; Yuan, S.; Wang, X.; Xu, T.; Wang, X.; Li, H.; Zheng, W.; Fan, P.; Li, Y.; Sun, L.; et al. Vapor Growth and Tunable Lasing of Band Gap Engineered Cesium Lead Halide Perovskite Micro/Nanorods with Triangular Cross Section. *ACS Nano* **2017**, *11*, 1189−1195.

(3) Yang, T.; Zheng, Y.; Du, Z.; Liu, W.; Yang, Z.; Gao, F.; Wang, L.; Chou, K. C.; Hou, X.; Yang, W. J. A. N. Superior Photodetectors Based on All-Inorganic Perovskite $CsPbI_3$ Nanorods with Ultrafast Response and High Stability. *ACS Nano* **2018**, *12*, 1611−1617.

(4) Luo, C.; Li, W.; Fu, J.; Yang, W. Constructing Gradient Energy Levels to Promote Exciton Energy Transfer for Photoluminescence Controllability of All-Inorganic Perovskites and Application in Single-Component WLEDs. *Chem. Mater.* **2019**, *31*, 5616−5624.

(5) Xie, M.; Liu, H.; Chun, F.; Deng, W.; Luo, C.; Zhu, Z.; Yang, M.; Li, Y.; Li, W.; Yan, W.; et al. Aqueous Phase Exfoliating Quasi-2D $CsPbBr_3$ Nanosheets with Ultrahigh Intrinsic Water Stability. *Small* **2019**, *15*, No. 1901994.

(6) Luo, C.; Yan, C.; Li, W.; Chun, F.; Xie, M.; Zhu, Z.; Gao, Y.; Guo, B.; Yang, W. Ultrafast Thermodynamic Control for Stable and Efficient Mixed Halide Perovskite Nanocrystals. *Adv. Funct. Mater.* **2020**, *30*, No. 2000026.

(7) Yakunin, S.; Protesescu, L.; Krieg, F.; Bodnarchuk, M. I.; Kovalenko, M. V.; et al. Low-threshold amplified spontaneous emission and lasing from colloidal nanocrystal of caesium lead halide perovskites. *Nat. Commun.* **2015**, *6*, No. 8056.

(8) Li, G.; Rivarola, F. W.; Davis, N. J.; Bai, S.; Jellicoe, T. C.; de la Pena, F.; Hou, S.; Ducati, C.; Gao, F.; Friend, R. H.; et al. Highly Efficient Perovskite Nanocrystal Light-Emitting Diodes Enabled by a Universal Crosslinking Method. *Adv. Mater.* **2016**, *28*, 3528−3534.

(9) Hou, S.; Gangishetty, M. K.; Quan, Q.; Congreve, D. N. Efficient Blue and White Perovskite Light-Emitting Diodes via Manganese Doping. *Joule* **2018**, *2*, 2421−2433.

(10) Xing, J.; Zhao, Y.; Askerka, M.; Quan, L. N.; Gong, X.; Zhao, W.; Zhao, J.; Tan, H.; Long, G.; Gao, L.; et al. Color-stable highly luminescent sky-blue perovskite light-emitting diodes. *Nat. Commun.* **2018**, *9*, No. 3541.

(11) Swarnkar, A.; Marshall, A. R.; Sanehira, E. M.; Chernomordik, B. D.; Moore, D. T.; Christians, J. A.; Chakrabarti, T.; Luther, J. M. J. S. Quantum dot-induced phase stabilization of alpha-$CsPbI_3$ perovskite for high-efficiency photovoltaics. *Science* **2016**, *354*, 92−95.

(12) Yuan, Y.; Li, T.; Wang, Q.; Xing, J.; Gruverman, A.; Huang, J. Anomalous photovoltaic effect in organic-inorganic hybrid perovskite solar cells. *Sci. Adv.* **2017**, *3*, No. e1602164.

(13) Lekina, Y.; Shen, Z. X. Excitonic states and structural stability in two-dimensional hybrid organic-inorganic perovskites. *J. Sci. Adv. Mater. Devices* **2019**, *4*, 189−200.

(14) Mao, L.; Stoumpos, C. C.; Kanatzidis, M. G. Two-Dimensional Hybrid Halide Perovskites: Principles and Promises. *J. Am. Chem. Soc.* **2019**, *141*, 1171−1190.

(15) Najer, D.; Sollner, I.; Sekatski, P.; Dolique, V.; Lobl, M. C.; Riedel, D.; Schott, R.; Starosielec, S.; Valentin, S. R.; Wieck, A. D.; et al. A gated quantum dot strongly coupled to an optical microcavity. *Nature* **2019**, *575*, 622−627.

(16) Li, J.; Luo, L.; Huang, H.; Ma, C.; Ye, Z.; Zeng, J.; He, H. 2D Behaviors of Excitons in Cesium Lead Halide Perovskite Nanoplatelets. *J. Phys. Chem. Lett.* **2017**, *8*, 1161−1168.

(17) Ma, Z.; Shi, Z.; Qin, C.; Cui, M.; Yang, D.; Wang, X.; Wang, L.; Ji, X.; Chen, X.; Sun, J.; et al. Stable Yellow Light-Emitting Devices Based on Ternary Copper Halides with Broadband Emissive Self-Trapped Excitons. *ACS Nano* **2020**, *14*, 4475−4486.

(18) Zeng, R.; Zhang, L.; Xue, Y.; Ke, B.; Zhao, Z.; Huang, D.; Wei, Q.; Zhou, W.; Zou, B. Highly Efficient Blue Emission from Self-Trapped Excitons in Stable Sb^{3+}-Doped $Cs_2NaInCl_6$ Double Perovskites. *J. Phys. Chem. Lett.* **2020**, *11*, 2053−2061.

(19) Sun, C.; Gao, Z.; Deng, Y.; Liu, H.; Wang, L.; Su, S.; Li, P.; Li, H.; Zhang, Z.; Bi, W. Orange to Red, Emission-Tunable Mn-Doped Two-Dimensional Perovskites with High Luminescence and Stability. *ACS Appl. Mater. Interfaces* **2019**, *11*, 34109−34116.
(20) Weidman, M. C.; Seitz, M.; Stranks, S. D.; Tisdale, W. A. J. A. N. Highly Tunable Colloidal Perovskite Nanoplatelets Through Variable Cation, Metal, and Halide Composition. *ACS Nano* **2016**, *10*, 7830−7839.
(21) Straus, D. B.; Kagan, C. R. Electrons, Excitons, and Phonons in Two-Dimensional Hybrid Perovskites: Connecting Structural, Optical, and Electronic Properties. *J. Phys. Chem. Lett.* **2018**, *9*, 1434−1447.
(22) Chen, J.; Shi, Y.; He, Y.; Zhai, T. Two-dimensional Ruddlesden-Popper perovskite nanosheets: Synthesis, optoelectronic properties and miniaturized optoelectronic devices. *FlatChem* **2019**, *17*, No. 100116.
(23) Yu, J.; Kong, J.; Hao, W.; Guo, X.; He, H.; Leow, W. R.; Liu, Z.; Cai, P.; Qian, G.; Li, S.; et al. Broadband Extrinsic Self-Trapped Exciton Emission in Sn-Doped 2D Lead-Halide Perovskites. *Adv. Mater.* **2019**, *31*, No. e1806385.
(24) Chen, X.; Lu, H.; Yang, Y.; Beard, M. C. Excitonic Effects in Methylammonium Lead Halide Perovskites. *J. Phys. Chem. Lett.* **2018**, *9*, 2595−2603.
(25) Blancon, J. C.; Stier, A. V.; Tsai, H.; Nie, W.; Stoumpos, C. C.; Traore, B.; Pedesseau, L.; Kepenekian, M.; Katsutani, F.; Noe, G. T.; et al. Scaling law for excitons in 2D perovskite quantum wells. *Nat. Commun.* **2018**, *9*, No. 2254.
(26) He, H.; Yu, Q.; Li, H.; Li, J.; Si, J.; Jin, Y.; Wang, N.; Wang, J.; He, J.; Wang, X.; et al. Exciton localization in solution-processed organolead trihalide perovskites. *Nat. Commun.* **2016**, *7*, No. 10896.
(27) Telfah, H.; Jamhawi, A.; Teunis, M. B.; Sardar, R.; Liu, J. Ultrafast Exciton Dynamics in Shape-Controlled Methylammonium Lead Bromide Perovskite Nanostructures: Effect of Quantum Confinement on Charge Carrier Recombination. *J. Phys. Chem. C* **2017**, *121*, 28556−28565.
(28) Grim, J. Q.; Christodoulou, S.; Stasio, F. D.; Krahne, R.; Cingolani, R.; Manna, L.; Moreels, I. J. N. N. Continuous-wave biexciton lasing at room temperature using solution-processed quantum wells. *Nat. Nanotechnol.* **2014**, *9*, 891−895.
(29) Hong, X.; Ishihara, T.; Nurmikko, A. V. Dielectric confinement effect on excitons in PbI_4-based layered semiconductors. *Phys. Rev. B* **1992**, *45*, 6961−6964.
(30) Liu, R. T.; Zhai, X. P.; Zhu, Z. Y.; Sun, B.; Liu, D. W.; Ma, B.; Zhang, Z. Q.; Sun, C. L.; Zhu, B. L.; Zhang, X. D.; et al. Disentangling the Luminescent Mechanism of Cs_4PbBr_6 Single Crystals from an Ultrafast Dynamics Perspective. *J. Phys. Chem. Lett.* **2019**, *10*, 6572−6577.
(31) Schmidt, T.; Lischka, K.; Zulehner, W. Excitation-power dependence of the near-band-edge photoluminescence of semiconductors. *Phys. Rev. B* **1992**, *45*, 8989−8994.
(32) McCall, K. M.; Stoumpos, C. C.; Kostina, S. S.; Kanatzidis, M. G.; Wessels, B. W. Strong Electron−Phonon Coupling and Self-Trapped Excitons in the Defect Halide Perovskites $A_3M_2I_9$ (A = Cs, Rb; M = Bi, Sb). *Chem. Mater.* **2017**, *29*, 4129−4145.
(33) Ni, L.; Huynh, U.; Cheminal, A.; Thomas, T. H.; Shivanna, R.; Hinrichsen, T. F.; Ahmad, S.; Sadhanala, A.; Rao, A. Real-Time Observation of Exciton-Phonon Coupling Dynamics in Self-Assembled Hybrid Perovskite Quantum Wells. *ACS Nano* **2017**, *11*, 10834−10843.
(34) Luo, B.; Liang, D.; Sun, S.; Xiao, Y.; Lian, X.; Li, X.; Li, M. D.; Huang, X. C.; Zhang, J. Z. Breaking Forbidden Transitions for Emission of Self-Trapped Excitons in Two Dimensional $(F_2CHCH_2NH_3)_2CdBr_4$ Perovskite through Pb Alloying. *J. Phys. Chem. Lett.* **2020**, *11*, 199−205.
(35) Luo, J.; Wang, X.; Li, S.; Liu, J.; Guo, Y.; Niu, G.; Yao, L.; Fu, Y.; Gao, L.; Dong, Q.; et al. Efficient and stable emission of warm-white light from lead-free halide double perovskites. *Nature* **2018**, *563*, 541−545.
(36) Wang, X. M.; Meng, W. W.; Liao, W. Q.; Wang, J. B.; Xiong, R. G.; Yan, Y. F. Atomistic Mechanism of Broadband Emission in Metal Halide Perovskites. *J. Phys. Chem. Lett.* **2019**, *10*, 501−506.
(37) Li, S.; Luo, J.; Liu, J.; Tang, J. Self-Trapped Excitons in All-Inorganic Halide Perovskites: Fundamentals, Status, and Potential Applications. *J. Phys. Chem. Lett.* **2019**, *10*, 1999−2007.
(38) Proppe, A. H.; Walters, G. W.; Alsalloum, A. Y.; Zhumekenov, A. A.; Mosconi, E.; Kelley, S. O.; De Angelis, F.; Adamska, L.; Umari, P.; Bakr, O. M.; et al. Transition Dipole Moments of n = 1, 2, and 3 Perovskite Quantum Wells from the Optical Stark Effect and Many-Body Perturbation Theory. *J. Phys. Chem. Lett.* **2020**, *11*, 716−723.
(39) Smith, M. D.; Karunadasa, H. I. White-Light Emission from Layered Halide Perovskites. *Acc. Chem. Res.* **2018**, *51*, 619−627.

https://dx.doi.org/10.1021/acs.jpcc.0c09334
J. Phys. Chem. C 2020, 124, 26076−26082